Corrosion Fatigue of Pressure Boundary Materials

F. P. FORD and P. L. ANDRESEN
General Electric Corporate Research and Development Center, River Road, Building K–1 Rooms 3A39/3A43, Schenectady, New York 12301, USA

ABSTRACT

The derivation of a model of environmentally-assisted cracking for ductile alloys in aqueous environments is described and applied to the formulation of life prediction codes for corrosion fatigue of austenitic stainless steel and low-alloy steels in 288°C water. These model predictions are compared with observed corrosion fatigue (and stress corrosion) data. It is concluded that the model more accurately predicts the effect of a wide range of material, environment and stressing conditions on crack propagation than does, e.g., the current (1980) ASME XI code.

KEYWORDS

Life prediction codes; corrosion fatigue; austenitic stainless steel; low alloy steel; slip dissolution.

INTRODUCTION

The 1980 ASME XI life evaluation code offers a methodology for determining the remaining life of defected iron-base structures undergoing fatigue loading in 288°C water. However, the data upon which this code is based is limited in terms of the frequency range, water chemistry conditions, etc., and does not cover the limiting condition of a static load when stress corrosion might occur. Over the past decade there has been extensive investigations of the mechanism of environmentally-assisted cracking (i.e., stress corrosion and corrosion fatigue) and how this fundamental knowledge may be applied *quantitatively* to a more complete formulation of the life prediction codes (Ford, Andresen, Taylor & Ballinger, 1987, Andresen & Ford, 1988, Cullen, 1985). The objective of this paper is to summarize the developments in mechanistic modeling of environmentally-assisted cracking of stainless steels and low-alloy (A533B/A508) steels commonly used as pressure boundary materials in e.g., Light Water Reactors, and to demonstrate the model validity and comparison with current life prediction codes for corrosion fatigue.

MODEL DERIVATION

The slip dissolution/film rupture mechanism of crack propagation was hypothesized for 304/316 stainless and A533B/A508 low-alloy steels in 288°C water (Ford, Andresen, Taylor & Ballinger, 1985). In this mechanism, Fig. 1, crack advance is related by Faraday's Law to oxidation reactions that occur at the crack tip as the protective film is ruptured by increasing strain in the underlying metal. Rupture occurs with a periodicity, t_f, which is calculated from the fracture strain of the oxide, ϵ_f, and the strain rate, $\dot{\epsilon}_{ct}$, at the crack tip. This behavior varies in a complex manner for different environment and material chemistries, although the crack propagation rate, V_T, can be formulated as:

$$V_T = \frac{M}{z\rho F} \frac{i_o t_o^n}{(1-n)\varepsilon_f^n} (\dot{\varepsilon}_{ct})^n \quad (1a)$$

$$\overline{V}_T = f(n)\,(\dot{\varepsilon}_{ct})^n \quad (1b)$$

where the various parameters, to be discussed later, relate to the kinetics of oxidation and oxide rupture. In general, however, the crack tip strain rate embodies the mechanical contributions and 'n' encompasses the effects of environment and material chemistries on the oxidation rates in the crack tip system.

There are limits to the validity of the crack growth rates predicted in Eqn. 1. At high crack tip strain rates ($\approx 10^{-2} s^{-1}$), a bare surface is maintained continuously at the crack tip, and the environmentally-assisted crack propagation rate becomes independent of the crack tip strain rate since it cannot exceed the Faradaic equivalent of the bare surface dissolution rate. Various phenomena can contribute to the lower validity limit for Eqn. 1. Historically, one such limiting phenomenon occurs when the crack tip propagation rate approaches the general corrosion rate on the crack sides and a sharp crack cannot be maintained. An overriding lower limit phenomenon is proposed in this paper for low-alloy steel that is associated with maintaining aggressive sulphur-rich species in the crack tip enclave as the advancing crack tip intersects dissolvable MnS inclusions; this phenomenon has also been examined by Combrade (1987).

Under constant or monotonically rising load conditions, the crack propagation rate is defined by Eqn. 1 (within the limits discussed above). Under cyclic loading conditions, the crack is also moving forward by irreversible plastic deformation. Since this mechanical crack advance occurs independently of the crack advance by oxidation processes, these two crack advance mechanisms are considered additive (Fig. 2). Thus, the working hypothesis addresses the full spectrum of stress corrosion and corrosion fatigue behavior.

To quantify this model, the following processes have to be defined:

1. The steady state and transient compositions of the environment at the crack tip as a function of that in the bulk (external) solution.

   On the basis of direct measurements for the stainless and low-alloy steel/water systems at 288°C, it is concluded that the electrode potential and anion activity at the occluded tip of a crevice/crack can differ markedly from those at the exposed crevice/crack mouth. The steady state variations in these values as a function of bulk solution parameters are understood in terms of the thermodynamics of various metal oxidation and metal cation hydrolysis reactions and how they are influenced by the mass transport kinetics in the crack. In the above work, these complex interactions have been distilled into relationships such as that in Fig. 3 which indicates the change in crack tip potential and pH with a measurable bulk solution parameter, dissolved oxygen content or corrosion potential.

   The transient and steady state concentration of anions in the crack were experimentally measured and analytically modeled (Ford, Andresen, Taylor & Ballinger, 1985, Andresen, 1987). The anion level present at the crack tip is strongly dependent on the external anionic activity, the metallurgical impurity (e.g., S) level, the corrosion potential difference between crack mouth and tip and convective influences. For instance, for stainless steel in stagnant solution, the increase in anion activity at the tip of a deep crack is directly related to the potential drop $\Delta\phi$ down the crack (shown in Fig. 3) via:

   $$C_{ct} = C_{bulk}(316)^{\Delta\phi} \quad (2)$$

   Thus, under aerated bulk solution conditions, the crack tip anionic activity may be increased by a factor of X100, but under deaerated conditions, the crack tip anion activity will approximate that in the bulk environment. A further criterion applies to low-alloy steels, however, since the dissolution of MnS inclusions offers a supply of sulphur rich anions as the crack front advances (Fig. 4). Thus, the crack tip sulphur concentration in the low-alloy steels may be related (Andresen, 1987, Ford & Andresen, 1989) to the crack velocity and the sulphur content of the steel, in addition to the normal mass transport criteria defined, for example, by Eqn. 2 (Fig. 5). Of significance to modelling of corrosion fatigue, is the experimental determination that convective effects due to the relative movement of the crack sides significantly affected the crack tip environment only under high ΔK and/or frequency conditions; under such conditions, the observed crack propagation rate is dominated by dry fatigue. Thus, convective transport due to cycling is of little practical importance. However, there are observed effects of the bulk solution flow rate on the steady state crack tip anion concentration and these are incorporated into the crack propagation model.

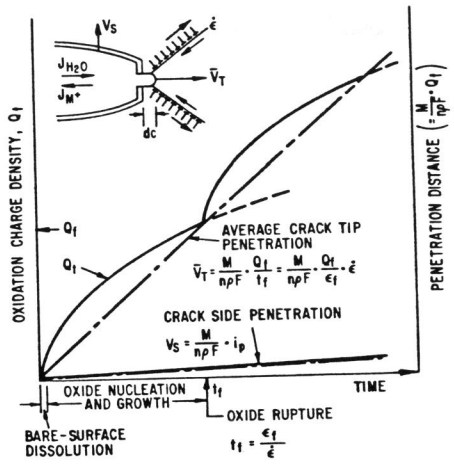

Fig. 1. Schematic of crack tip reactions pertinent to the slip dissolution/film rupture model of crack propagation.

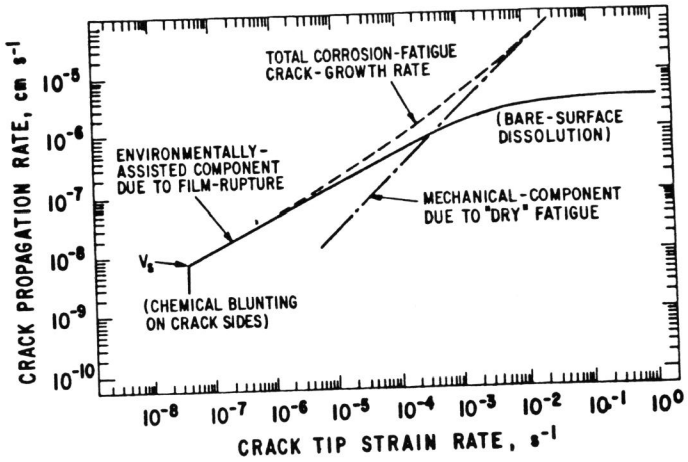

Fig. 2. Crack propagation rate/crack tip strain relationship according to slip dissolution model indicating the superposition of the environmental and mechanical (inert environment) components in corrosion fatigue.

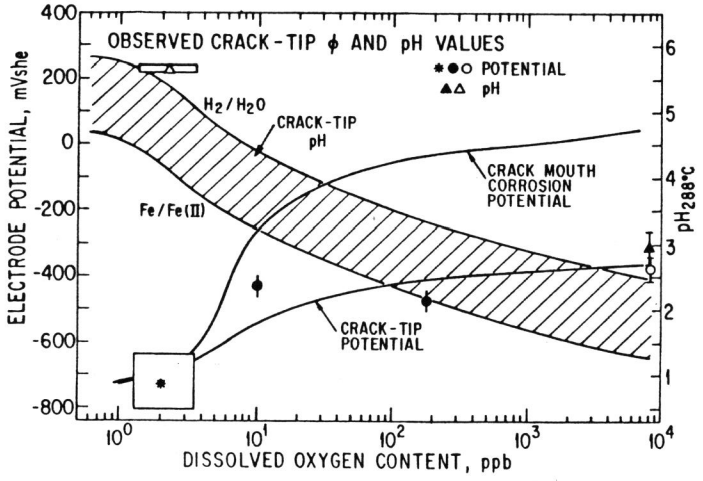

Fig. 3. Variation of crack tip potential and pH for stainless and low-alloy steels in 288°C water, as a function of the dissolved oxygen content in the bulk solution.

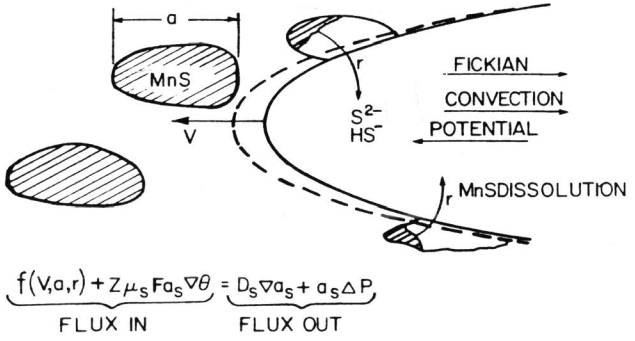

Fig. 4. The mass balance relationship for sulphur-rich anions at the crack tip, where such species are being introduced via dissolution of MnS inclusions which are being exposed by the advancing crack front.

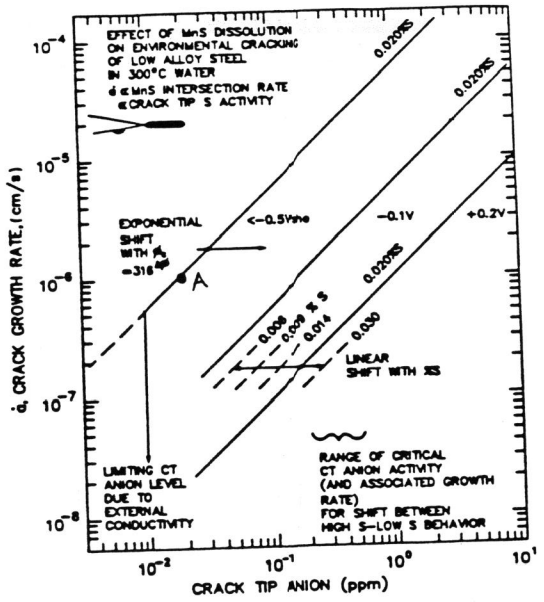

Fig. 5. Relationship between dissolved sulphur concentration at crack tip and the crack propagation rate for various sulphur contents in the steel and corrosion potential.

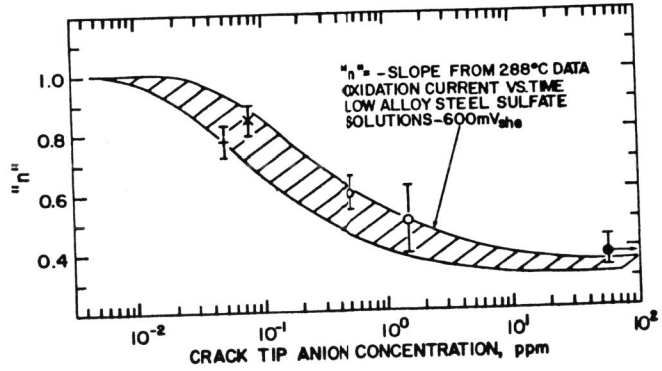

Fig. 6. Relationship between "n", the power law factor in Eqn. 3 for low-alloy steels, and the dissolved sulphur content at the crack tip.

2. The oxidation rates for the various material and environment conditions at a strained crack tip.

   The oxidation rates for material/environment systems characteristic of crack tips in stainless and pressure vessel steels in Light Water Reactors were measured in order to quantify the relationships which are shown schematically in Fig. 1. It was observed that the bare surface dissolution rate, i_o, decayed after a time, t_o, due to passivation processes (Ford, Andresen, Taylor & Ballinger, 1985), via power law of the form:

$$i_t = i_o \left(t / t_o\right)^{-n} \tag{3}$$

   where the value of i_o and t_o and n were functions of the material composition, anion content and potential pH. For instance, for potentials and pH expected at the crack tip, the value of n (which is the same parameter as in Eqn. 1) varies with crack tip anion content (Fig. 6); similar curves exist for different alloy composition, symptomatic of those expected at, for instance, a chromium denuded, nickel enriched, grain boundary. Various mechanistic reasons for such a dependency of the oxidation rate in high temperature water on the anion concentration have been advanced (Combrade, 1987, Andresen, 1987). Regardless of these specific details, however, the fact remains that by combining such independently derived values of n with the crack tip environment characterizations shown in Fig. 5 and Eqn. 2, the crack propagation rate/crack tip strain rate relationship (Fig. 2) may be derived.

3. The oxide fracture strain and crack tip strain rate.

   The crack tip strain rate determines the periodicity at which slip induced film rupture occurs and thus is *fundamentally* important, unlike the classical design parameters of residual and applied stress, stress intensity, loading frequency, etc. Several reviews have been published of the approaches used to formulate this parameter in terms of engineering parameters (Lidbury, 1984, Ford, Andresen, Taylor & Ballinger, 1985, Cullen, 1985). Such formulations all leave much to be desired, primarily because of the assumptions made and the relative lack of experimental verification under plain strain conditions. In the present work, the following formulations have been used (Ford, Andresen, Taylor & Ballinger, 1985) and the reader is referred to the above reviews for background information.

Table 1. Crack Tip Strain Rate Formulations for Stress Corrosion and Corrosion Fatigue

Constant Load	$\dot{\varepsilon}_{ct}$	$= 6 \times 10^{-14} K^4$ for stainless steel
		$= 4.8 \times 10^{-13} K^4$ for low-alloy steel
Cyclic Load	$\dot{\varepsilon}_{ct}$	$= 100 A_R \nu \Delta K^4$ for stainless steel
		$= 800 A_R \nu \Delta K^4$ for low-alloy steel
where	K, ΔK	= stress intensity (amplitude), $ksi\sqrt{in}$
	ν	= loading frequency, Hz
	A_R	= parameter which is function of R, the mean stress ratio

MODEL VALIDITY & COMPARISON WITH EXISTING LIFE PREDICTION CODES

The theoretical and observed crack propagation rate/crack tip strain rate relationships for sensitized 304 stainless steel in 288°C water are shown in Fig. 7 for two limiting environmental conditions. One relationship corresponds to observed stress corrosion (✗) and corrosion fatigue (●) data (Ford, Andresen, Taylor & Ballinger, 1985) obtained in 8 ppm oxygenated water, with the corresponding theoretical relationship computed on the basis of knowledge of oxidation kinetics in the crack tip material/environment system as described above. The other relationship corresponds to stress corrosion (◕) corrosion fatigue (○) data obtained in deaerated, high purity water at 288°C. In both cases it is seen that stress corrosion and corrosion fatigue data can be represented on the same time-base relationship, and that the propagation rates are in good agreement with the theoretical predictions. Indeed, when examining a much larger data base (340) covering a wide range of combinations of material, environment and stressing conditions, it is concluded that the *mean* calculated crack propagation rate is within 17% of the observed value (Ford, Andresen, Taylor & Ballinger, 1985).

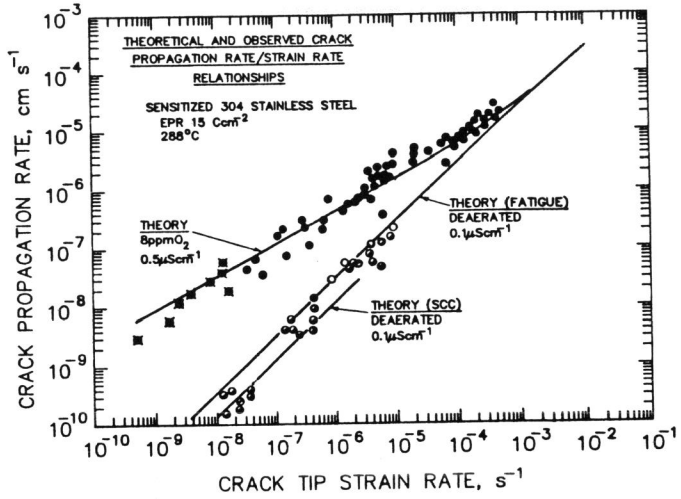

Fig. 7. Comparison between observed and theoretical crack propagation rate/crack tip strain relationships for sensitized 304 stainless steel in 288°C water, which is either aerated (8 ppm O_2) or deaerated.

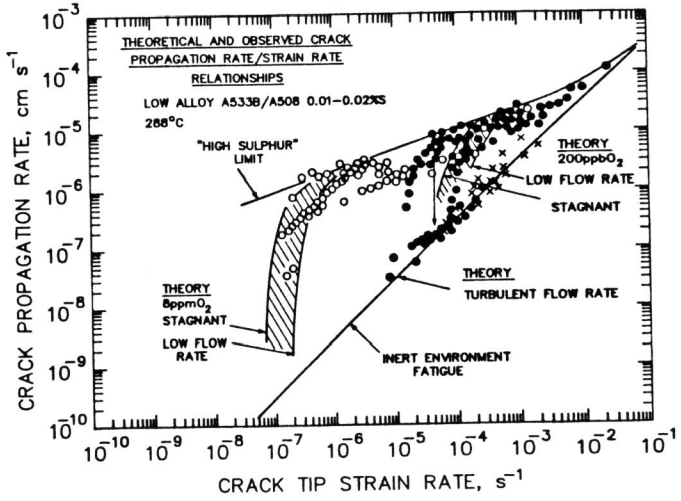

Fig. 8. Comparison between observed and theoretical crack propagation rate/crack tip strain rate relationships for low-alloy A533/A508 steels in 288°C water under various conditions of solution flow rate and dissolved oxygen content.

For sake of brevity, continued discussion is centered on environmentally-assisted cracking of low-alloy steels in 288°C. A representative comparison between the theoretical and observed propagation rate/crack tip strain rate relationships are shown in Fig. 8 for specific environment systems. It is seen that the shapes of these relationships differ from those for stainless steel (Fig. 7) because of the fact that the anion content of the crack tip (and, hence, the oxidation rate), is dominated by the continued intersection of dissolvable MnS inclusions by the advancing crack tip. Thus, enhanced crack propagation according to the "high sulphur limit" line in Fig. 8 continues until the crack propagation rate is no longer fast enough to maintain the high sulphur anionic activity. This critical condition will depend on the environmental condition, as illustrated in Fig. 8, for both stagnant and low flow rate 8 ppm oxygenated (O) and 200 ppb (●) water and turbulent flow deaerated water (×).

Further analysis of such data is confined to corrosion fatigue, although a similar analysis of stress corrosion behavior, per se, may be undertaken (Ford & Andresen, 1989). The time dependent data which is central to the model and data sets in Figs. 7 and 8 may be converted to cyclic-base crack growth rate via:

$$\left(\frac{da}{dN}\right)_{total} = \frac{1}{2\nu}\left[f(n)\,(\dot{\varepsilon}_{ct})^n\right] + \left(\frac{da}{dN}\right)_{inert} \qquad (4)$$

where the first term on the right hand side is the environmental component of crack advance (Eqn. 1) assuming that this only occurs during the rising portion of the loading cycle, and the second term is the mechanical fatigue component observed in an inert environment.

The da/dN vs. ΔK relationships for an A533B/A508 steel in stagnant/low flow rate deaerated water at 288°C are shown in Fig. 9 for an R value (= min/max stress) of 0.7. Also shown are the da/dN values for inert environment and the ASME XI 1980 code values for $R \geq 0.65$. The theoretical curves are shown for a range of sulphur content in the steel (0.005-0.02%) since this will determine the ease with which the "high sulphur anionic activity" at the crack tip is maintained. A significant number of corrosion fatigue data has been accumulated under the auspices of the International Cyclic Crack Growth Rate group (Cullen, 1985, Van der Sluys, 1985), and a representative set is shown in Fig. 10 for a cyclic frequency of 0.0167 Hz and R = 0.7. These data were obtained on steels with sulphur contents in the range 0.01-0.025% S. It is seen that the theoretical da/dN vs. ΔK relationships for such conditions are in reasonable agreement with these observed data. Further comparison between observation and theory is shown in Fig. 11 which examines the specific effects of loading frequency on the cyclic crack growth rate at $\Delta K = 22\ MPa\sqrt{m}$. Of significance is the fact that the da/dN values are observed and predicted to increase with decreasing frequency to a limit (which is a function of the sulphur content of the steel) when the high anionic sulphur activity cannot be maintained at the advancing crack front.

The conclusion at this stage is that the theory gives a reasonable prediction of the observed changes in da/dN values in deaerated water with changes in stress intensity amplitude and frequency. It is significant, however, that although the current ASME XI (1980) code approach gives a reasonable upper bound value of the da/dN value (at least for frequencies $\geq 10^{-2}$ Hz), it does not account for the specific frequency or sulphur content effects, per se.

The effect of oxygenation of the water on the corrosion fatigue behavior is shown in Figs. 12-14. Again, a reasonable correlation between observation and theory is noted in Figs. 13 and 14. As in deaerated environments, it is apparent that the observed frequency effects on the da/dN values are not accounted for by the current ASME XI code, nor is the deleterious effect of an oxidizing environment. Indeed, on the latter point, the current code may underpredict the cyclic crack growth rates in high sulphur content steels at lower stress intensity amplitude conditions (Fig. 12).

Finally, critical stress intensity/loading frequency combinations are predicted below which steady state environmental enhancement of fatigue crack growth will not be observed because the required dissolved sulphur anion content cannot be maintained by the advancing crack tip. These critical ΔK/frequency combinations will depend on the sulphur content of the steel, the dissolved oxygen content, and the flow rate of the bulk solution, since these will all control the mass transport of sulphur rich anions out of the crack. The observed ΔK/frequency combinations are shown in Fig. 15 for various sulphur content steels in stagnant/low flow rate water which was either aerated (200-300 ppb O_2) or deaerated; these observed data are successfully bounded by the theoretical relationships which correspond to the limits of the system conditions.

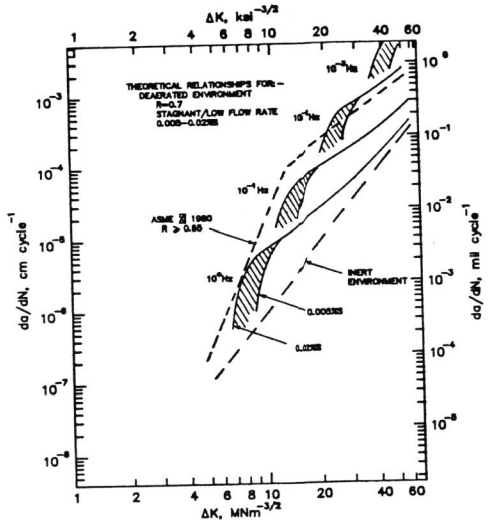

Fig. 9. Theoretical da/dN vs. ΔK relationships for A533/A508 steels in deaerated water when stressed at various frequencies at R = 0.7.

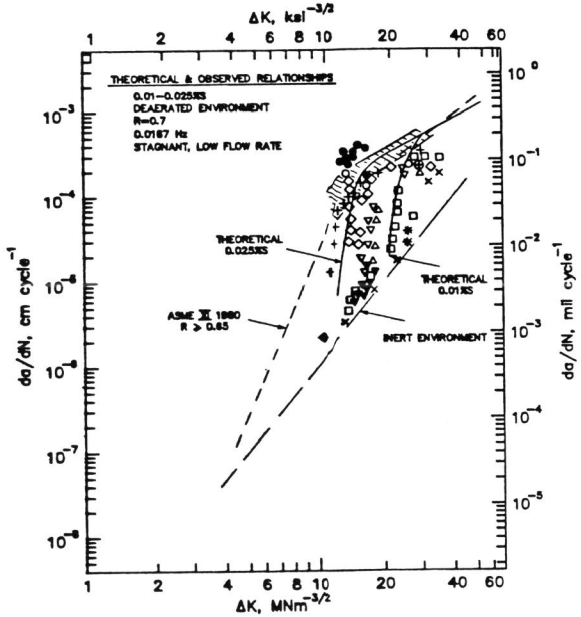

Fig. 10. Comparison between theoretical and observed da/dN vs. ΔK relationships for A533B/A508 steels with 0.01-0.025%S in deaerated water at 0.0167 Hz and R = 0.7.

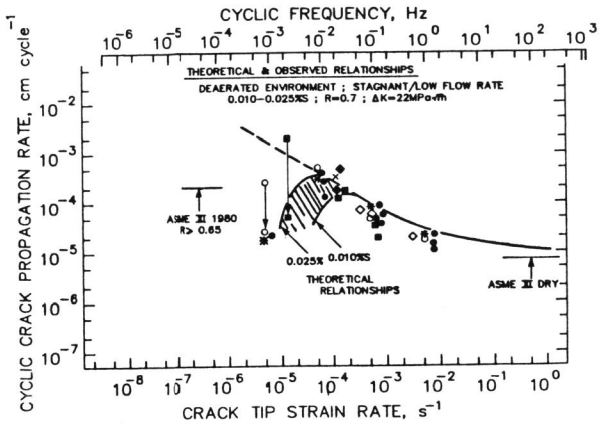

Fig. 11. Comparison between theoretical and observed da/dN vs. loading frequency relationships for A533B/A508 steels with 0.10-0.015% S in deaerated water at $\Delta K = 22\,MPa\sqrt{m}$ and R = 0.7.

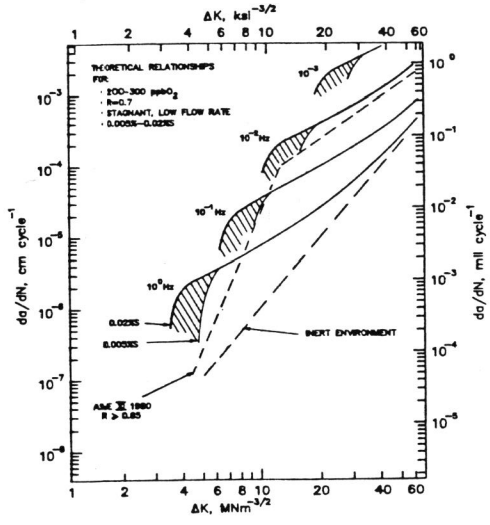

Fig. 12. Theoretical da/dN vs. ΔK relationships for A533/A508 steels in 200-300 ppb O_2 water when stressed at various frequencies and R = 0.7.

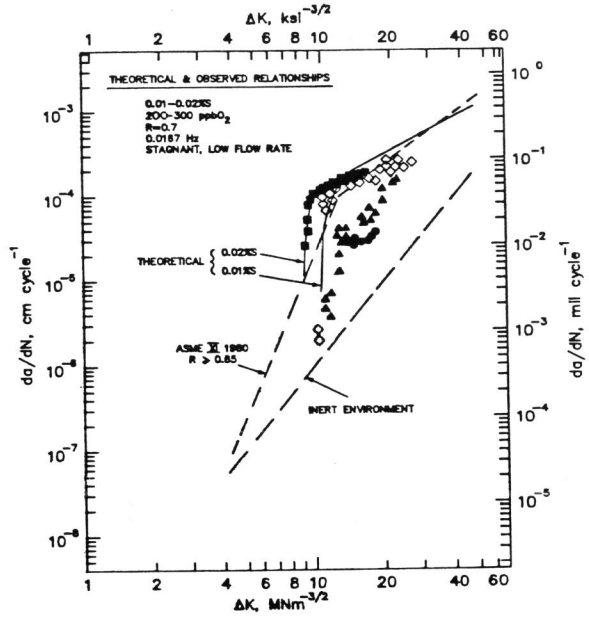

Fig. 13. Comparison between theoretical and observed da/dN vs. ΔK relationships for A533B/A508 steels with 0.01-0.025%S in 200-300 ppb O_2 water at 0.0167 Hz and R = 0.7.

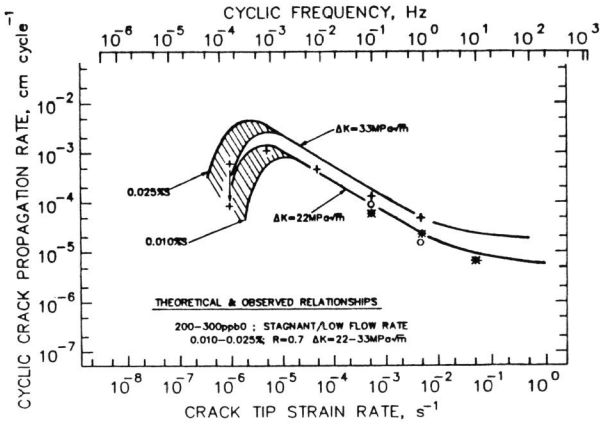

Fig. 14. Comparison between theoretical and observed da/dN vs. loading frequency relationships for A533B/A508 steels with 0.010-0.025%S in 200-300 ppb O_2 water, $\Delta K = 22\,MPa\sqrt{m}$ and R = 0.7.

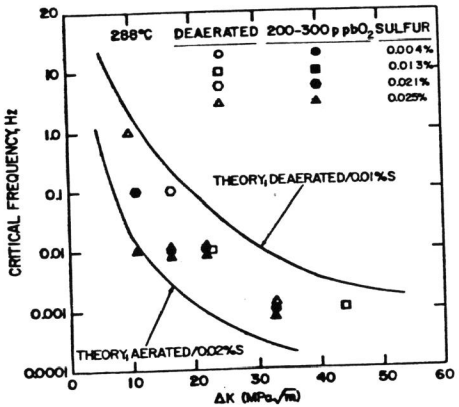

Fig. 15. Theoretical and observed (Van der Sluys, 1985), effects of ΔK, sulphur content in the steel, and oxygen content on the critical loading frequency below which environmental enhancement cannot be maintained. Theoretical curves shown for limiting combinations of oxygen content and sulphur content.

CONCLUSIONS

It is concluded that quantitative mechanistic understanding of environmentally-assisted crack propagation processes can offer valuable practical help to the designer and operational engineer. In particular, it is demonstrated that such understanding leads to a predictive capability for corrosion fatigue of stainless and low-alloy steels subjected to corrosion fatigue in 288°C water. Moreover, this knowledge correctly predicts the effects of material (sensitization, sulphur content), environment (oxygen content) and stressing conditions (frequency) on corrosion fatigue which are *not* factors in the, e.g., current ASME XI life evaluation code.

REFERENCES

P. Andresen (1987). Modeling of Water & Material Chemistry Effects on Crack Tip Chemistry, Proc. of Third Symp. on *Environmental Degradation of Materials in Nuclear Power Systems*, Traverse City, ANS/AIME/NACE (1987).

P. Andresen & P. Ford (1988). Life Prediction by Mechanistic Modeling & System Monitoring of Environmental Cracking of Iron and Nickel Alloys in Aqueous Systems, Mat. Sci. & Eng., A103, 167-184 (1988).

P. Combrade, M. Foucault & G. Slama (1987). Effect of Sulphur on Fatigue Crack Growth Rates of Pressure Vessel Steel Exposed to PWR Coolant, as Andresen (1987).

W. Cullen (1985). Proc., 2nd IAEA Specialists Meeting on Subcritical Crack Growth, Sendai, Japan, May 15-17, 1985. NUREG documents CP0067, Vols. 1 and 2.

P. Ford, P. Andresen, D. Taylor & R. Ballinger (1987). Corrosion Assisted Cracking of Stainless and Low-Alloy Steels in LWR Environments, EPRI Report NP50645, Feb. 1987.

P. Ford & P. Andresen (1989). Stress Corrosion Cracking of Low-Alloy Steels in 288°C Water, Paper #498, Corrosion/89, New Orleans, NACE, April 1989.

D. Lidbury (1983). The Calculation of Crack Tip Strain Rate Parameters Characterizing Environment Assisted Crack Growth Rate. Proc. AIME Conf., *Enbrittlement by the Localized Crack Environment*. Ed. R. Gangloff, Philadelphia, October 4-5, 1983.

A. Van der Sluys (1985). Overview of Data Trends in Cydic Crack Growth Results in LWR Environments, as Cullen (1985), Vol. 1, pp. 199-218.